Computational Materials Science 225 (2023) 112195

Contents lists available at ScienceDirect

Computational Materials Science

journal homepage: www.elsevier.com/locate/commatsci

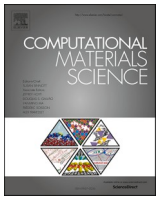

Full Length Article

Transition between a nano-sized prismatic dislocation loop and vacancy cluster in α-iron: An atomic scale study

Mugilgeethan VIJENDRAN [a,b,*], Ryosuke MATSUMOTO [a]

[a] Department of Mechanical and Electrical Systems Engineering, Kyoto University of Advanced Science, 18, Yamanouchi-Gotandacho, Ukyo-word, Kyoto 615-8577 Japan

[b] Faculty of Engineering, University of Jaffna, Ariviyal Nagar, Kilinochchi 44000, Sri Lanka

ARTICLE INFO

Keywords:
Prismatic dislocation loop
Molecular statics simulations
Iron
Vacancies
Activation energy
Transition

ABSTRACT

Plastic deformation and the presence of hydrogen enhance the concentration of vacancy-type defects in α-iron, wherein monovacancies can accumulate as a planar vacancy cluster (VC). The planar VC can then be nucleated into a corresponding prismatic dislocation loop (PDL), which can also be directly generated through cross-slip mechanisms of a screw dislocation. Inversely, a PDL can be converted to a corresponding VC. High densities of VCs and PDLs can significantly influence the mechanical properties of iron-based materials. Here, a quantitative energy barrier is established for the transition between nano-sized 1/2 ⟨111⟩ PDLs and VCs using the nudged elastic band method for different applied strains. It was concluded that a cluster size of more than 19 vacancies can easily nucleate into a PDL if a VC with planar configuration is formed in α-iron. Further, the nano-sized VC to PDL transition is enhanced under compressive strain while the nano-sized PDL to VC transition is enhanced under tensile strain. This result indicates that nano-sized VCs generated by tensile deformation are converted to a PDL after unloading and diffusing away. Inversely, nano-sized PDLs that form by deformation can easily diffuse to high tensile stress regions near stress singularities, such as crack tips and triple-junctions of grain boundaries, and then accumulate as high-density VCs.

1. Introduction

Hydrogen (H) is a sustainable energy carrier/source that plays a vital role in future energy demand [1,2]. However, development of H as an alternative energy carrier/source is highly influenced by its effective distribution [3]. Low-alloy steel is a potential material for hydrogen storage and transport because of its balance between cost and strength. However, the presence of H in steel causes hydrogen embrittlement (HE). The HE effects on the mechanical properties of structural metals have been well recognized for over a century and often lead to premature failure [4]. Thus, HE has been an essential issue that is particularly severe in steels because of the high mobility of H in iron (Fe) [5]. α-iron represents the simplest model to study HE due to the absence of impurities, which complicate the interpretation of empirical results and numerical simulation. Various mechanisms have been proposed to explain the origin of the embrittlement process, such as hydrogen-enhanced DEcohesion (HEDE) [6], hydrogen-enhanced localized plasticity (HELP) [7], and hydrogen-enhanced strain-induced vacancy (HESIV) [8]. However, problems related to HE still remain unsolved [9].

Recent studies have proposed that dislocations, stacking faults, and atomic vacancies are potential HE controlling factors [4]. Notably, recent studies have shown that H facilitates the formation of monovacancies and small vacancy clusters (VCs), such as di- and tri-vacancies, which lead to the formation of more vacancy–hydrogen complexes or larger VCs. Further, according to the study as the size of a VC increases, the mobility of the cluster decreases. This means that H atoms trapped in the cluster are less likely to move from one vacancy to another. Instead, H diffusion is likely to occur through dissociation, wherein H atoms separate from the cluster and move independently [10]. It has also been observed that hydrogen is released by aging in an H-free environment at room temperature, which leaves the monovacancies to aggregate into clusters or to disappear [11].

Abbreviations: BCC, Body-centered cubic; CG, Conjugate gradient; GB, Grain boundaries; HE, Hydrogen embrittlement; LAMMPS, Large-scale atomic/molecular massively parallel simulator; MD, Molecular dynamics; NEB, Nudged elastic band; PDL, Prismatic dislocation loop; SIA, Self-interstitial atom; TJGB, Triple junction of grain boundaries; VC, Vacancy cluster.

* Corresponding author.
E-mail addresses: mugil@eng.jfn.ac.lk (M. VIJENDRAN), matsumoto.ryosuke@kuas.ac.jp (R. MATSUMOTO).

https://doi.org/10.1016/j.commatsci.2023.112195
Received 24 November 2022; Received in revised form 27 March 2023; Accepted 9 April 2023
Available online 20 April 2023

When a planar VC is sufficiently large, the Fe atoms on both top and bottom inner sides of the VC collapse into each other by the attractive force between opposing atoms. As a result, a vacancy-type prismatic dislocation loop (PDL) is formed. The Burgers vector of a 1/2 ⟨1 1 1⟩ PDL in iron is highly mobile and can be easily glided along the direction of Burgers vector [12–15]. Many recent investigations have focused on the formation and stability of interstitial and vacancy-type PDLs in irradiated body-centered cubic (BCC) Fe, which is a suitable material for future fusion reactors. Fikar et al. investigated the energies of PDLs with different shapes and Burgers vectors, discovering that the 1/2 ⟨1 1 1⟩ regular hexagon shaped PDL is the most stable configuration [16]. The clustering in the cascade region based on the molecular dynamics study presents that up to 50 SIA are stable cluster in bcc-Fe and it can be describe as edge dislocation loops in the {1 1 1} plane [17]. Relaxed dislocation loop formation energies were also compared by considering larger interstitial defects. An extensive simulation study of the structure and energetics of self-interstitial atom (SIA) clusters and PDLs in pure BCC iron were studied for clusters containing up to 91 SIAs [18]. A new scaling law to account for the effect of temperature on the formation energy has been established for the free energies of SIA-type PDLs up to 30-nm in diameter at 1100 K [19]. The study presents that a single layer platelet containing upto 37 vacancies in bcc crystal does not nucleated to a dislocation loop in a static simulation. Further, the most stable structure is found to be compact vacancy clusters, followed by double layers, linear layers, linear chains, tetravacancies, single layers, trivacancies, and divacancies [20]. The study based on molecular dynamics of collapse of vacancy clusters mainly voids presented that vacancy loops with burgers vector b = ⟨1 0 0⟩ may form directly in bcc metals by cascade collapse on (1 0 0) planes, rather than by collapse on {1 1 0}. Further, simulation of void collapse reports that ½⟨1 1 1⟩ type Frank loop formed but it has defect of three-dimensional character [21]. The recent study comparing the formation energy of void, vacancy clusters formed in cascade and prismatic vacancy loop in bcc-tungsten is compared using molecular static simulation and fitting function. The transformation between a 3D void and a vacancy dislocation loop involves diffusion with the movement of many atoms [22].

Intergranular (IG), transgranular, and quasi-cleavage fractures have been widely recognized as HE fractures in steels [23–25]. Recent experimental observations have reported that damage resulting from clustering vacancies is closely associated with intense strain localization at the vicinity of grain boundaries (GBs) [26]. A recent study presented that the existence of critical vacancy concentration acts as a threshold for the entire IG fracture and facilitates quantitative prediction of HE in polycrystalline materials [27]. More significantly, consideration was given mainly to the formation of an SIA cluster and the corresponding PDL. It is also important to clarify the formation mechanisms of VCs at a small scale and the energy barrier necessary to comprehend the transitions of VCs and PDLs. In light of these recent findings, our study focuses on understanding the process by which VCs nucleate into PDL after H release. Therefore, we examine the behavior of VCs and their transformation into PDL without considering the impact of H.

The present study clarifies the formation mechanism of symmetrical and elongated hexagonal planar VCs and the corresponding 1/2 ⟨1 1 1⟩ PDL (Section 3). Furthermore, the activation energy associated with the transition from VCs to the PDL (and vice versa) with and without tensile/compressive strain is clarified (Section 4). Much attention was given to smaller VCs, those formed by less than 91 vacancies, where the VC to PDL transition is more likely to occur. Based on the simulation results, we propose a high-speed vacancy transportation mechanism, from compressive to tensile strain regions.

2. Simulation model and methodology

The computational analysis presented in this paper employed a bulk-like rectangular simulation block with periodic boundary conditions in all directions. The analyses were performed with the large-scale atomic/molecular massively parallel simulator (LAMMPS), which is open-source software for molecular dynamics (MD) simulation [28]. In order to describe the Fe–Fe interaction, an embedded atom method potential developed by Wen was applied in this work [29]. This potential was developed using the Fe–Fe model of the Ackland-2004 empirical potential [30]. The Ackland-2004 potential satisfactorily represents the properties of dislocations and dislocation loops in Fe [31].

As shown in Fig. 1, the simulation model was created with single-crystal α-iron containing $N = 1,710,720$ Fe atoms with dimensions of 25.18 nm, 24.24 nm, and 32.64 nm along x, y, and z directions, with $[2\bar{1}\bar{1}]$, $[01\bar{1}]$, and [111], respectively (Fig. 1(a)). This model represents a good tradeoff between avoiding spurious interaction with periodic images and an affordable computational cost. The planar VC is generated by removing atoms on the {1 1 1} plane (Fig. 1(b)). Hereafter, we denote a VC consisting of n vacancies as Vn. Fig. 1 (c) and (d) depict models of single- and three-layer V19 in the {1 1 1} plane. In the case of a single-layer cluster, the top and bottom layers of the platelets always tend to draw away from each other at the center of the platelet, where it should undergo plane translation motion to nucleate as a corresponding PDL. Therefore, nucleation of a PDL from a smaller VC is difficult for single-layer VCs. Accordingly, the study focused on three-layer clusters and did not consider the single-layer cluster in the analysis. The symmetrical or elongated hexagonal shape was removed by considering three layers in preparation of three-layer VCs for the {1 1 1} plane, as shown in Fig. 1 (d).

Vn_i is introduced in the {1 1 1} plane, where n_i is expressed by $n_i = 3i(i+1)+1$ and i denotes the order of symmetrical hexagonal-shaped VCs. In this paper, $2 \leq i \leq 10$ is investigated. For $i = 1$, the shape of the VC becomes a pillar with a triangle base, rather than a planar VC, and it is difficult to generate a PDL unless under large compressive strain (> 3%). Furthermore, V29 (an elongated hexagonal shape VC) was considered for analyzing the transition between a VC and PDL under applied strain. After removing atoms to create the VC, axial strain along the z direction is homogeneously applied, the atomic positions are relaxed using the conjugate gradient (CG) method, and the formation energy of the VC or PDL is then calculated. The formation energy, $E_{f,n_i}(\varepsilon)$, of a VC or PDL is computed using

$$E_{f,n_i}(\varepsilon) = E_{n_i}(\varepsilon) - (N - n_i) \times E_{Fe}(\varepsilon) \quad (1)$$

where $E_{n_i}(\varepsilon)$ is the relaxed total energy of the model for a VC or PDL consisting of n_i vacancies under strain ε and $E_{Fe}(\varepsilon)$ is the energy of an Fe atom in bulk perfect crystal under strain ε.

Different from SIA-type clusters, the smaller planar VCs usually do not nucleate to the corresponding PDL. Therefore, a large initial compressive strain was given to generate small PDLs for $N_i \leq 169$. Next, the intended strain was applied and atomic positions were relaxed. We successfully obtained PDLs at zero strain for $N_i \geq 19$. For $19 \leq N_i \leq 169$, both the VC and PDL can stably exist under zero strain and 0 K as shown in Section 3, which is quite a unique characteristic compared to SIA-type clusters. V19 is the smallest VC or PDL treated in this paper, and its height is close to its base-edge length. V19 is a stable structure with high symmetricity and, thus, when a VC grows it transition through the V19 with high probability.

The energy barriers for the transition between a VC and PDL were calculated using the nudged elastic band (NEB) method for $19 \leq N_i \leq 169$. Initial and final states for the NEB calculations were prepared carefully with the abovementioned procedures. NEB calculations were performed using 12 to 40 intermediate images to discretize the minimum energy pathway. All images had the same cell dimensions based on the initial state, which includes the VC. The energy barrier of a transition from VC to PDL (or from PDL to VC) is extracted as the difference in energy between the initial (or final) state and the highest energy state of the pathway, which corresponds to the transition state.

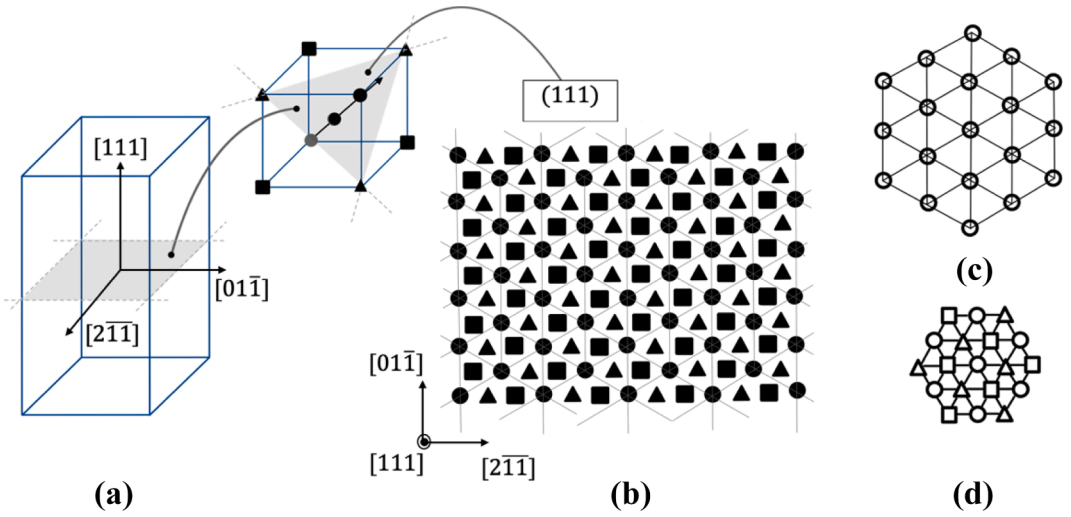

Fig. 1. (a) Simulation model and (b) three-layer slab of the (1 1 1) plane where ●, ■, and ▲ indicate atoms in the different layers; (1 1 1) (c) single-layer and (d) three-layer V19 VC (○, □, and Δ express the vacancy in the different layers).

3. Formation energy of a VC and PDL

The formation energies, E_{f,N_i}, of a VC and PDL under 0 % strain and contact surface area A_{V_i}, expressed as $A_{V_i} = 3\sqrt{3}/2[(i+1) \times d_{<110>}/2]^2$, where $d_{<110>}$ is the atomic distance along the ⟨1 1 0⟩ direction (also see Fig. 2(a)), are summarized in Table 1. A_{V_i} was calculated by assuming a regular hexagonal shape for the upper or bottom surface of a VC. The formation energies of V19, V61, and V91 are 24.74, 74.19, and 109.47 eV, respectively. The values are consistent up to V61 [32] and stable compared to SIA-type clusters consisting of 19 and 91 SIAs, which are 43.7 and 116.8 eV, respectively [18]. As depicted in Fig. 2, the energy of a planar VC is almost proportional to the upper and lower surface area of the cluster, i.e., it is proportional to i^2.

On the other hand, the energy of a PDL is almost proportional to the dislocation length, i.e., it is proportional to i (Fig. 2(b)).

Thus, for a larger VC (or larger i), the transition to a PDL occurs. The PDL dislocation length was computed by employing the DXA modifier, which generates the dislocation length using the Burgers vector conservation rule [33].

Table 1
Formation energy of prismatic dislocation loops (PDLs) and vacancy clusters (VCs) for selected VC sizes at zero strain with computed surface area.

VC size	A_{V_i} (nm^2)	$E_{f,MS}(VC)$ (eV)	$E_{f,MS}(PDL)$ (eV)
19	1.27	24.74	26.10
37	2.26	46.14	43.02
61	3.53	74.19	62.16
91	5.08	109.48	82.99
127	6.92	150.93	105.02
169	9.03	198.94	128.16
217	11.43	–	151.81
271	14.12	–	176.32
331	17.08	–	201.32

Fig. 3 shows a plot of the formation energy of the VC or corresponding PDL for different sizes. As shown by solid lines in Fig. 3(a), the formation energy increases monotonically as the vacancy number increases to a specific size. However, in the case of 0 % strain, a downshift

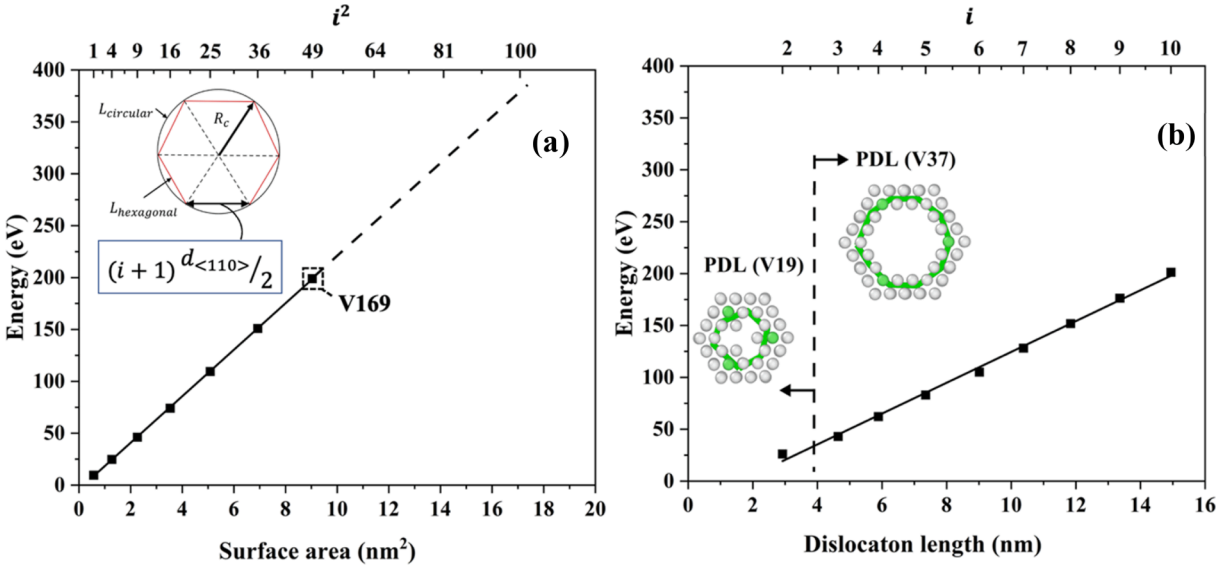

Fig. 2. Comparison of PDL formation energy without strain (a) as a function of surface area of the top and bottom cluster layers and i^2 and (b) as a function of dislocation length and i.

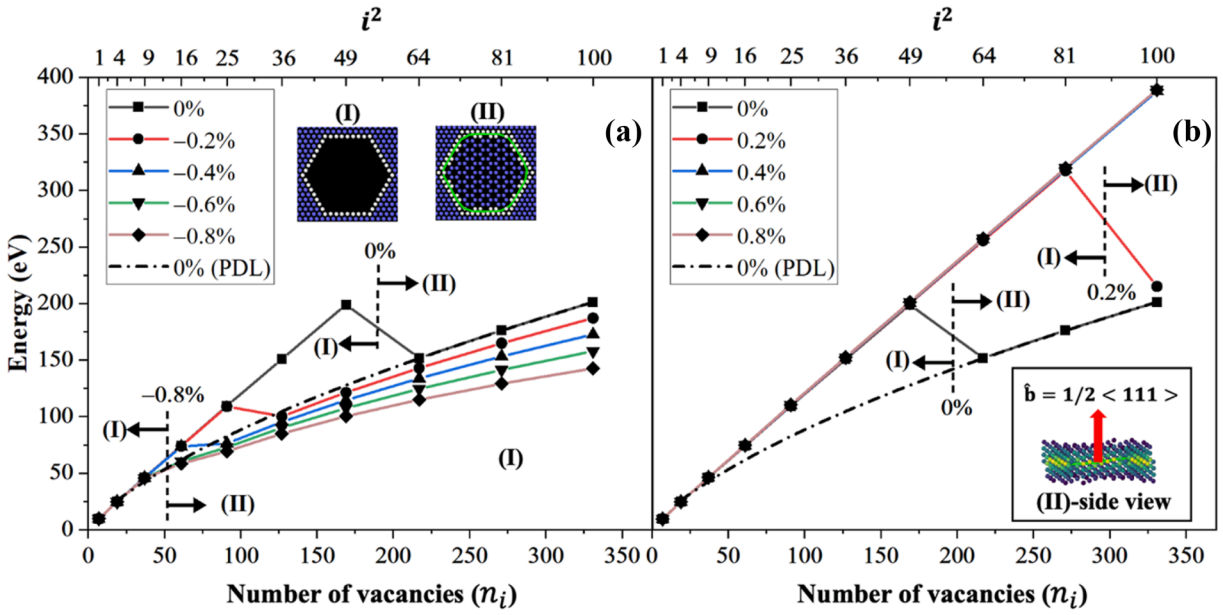

Fig. 3. VC formation energy as a function of loop size for different values of applied strain: (a) compressive strain and (b) tensile strain.

can be noticed when the vacancy number reaches 217, where the cluster nucleates into a corresponding PDL after energy minimization. As the number of vacancies increases, the related surface area inside of the VC increases, facilitating atomic binding between the top and bottom layers of the VC. Further, downshift was enhanced as the compressive strain increased. At 0.8 % compressive strain for V61 and larger, the VCs nucleated as a PDL and the remaining VCs stayed as clusters. Whereas, under tensile strain, the behavior is entirely different. At 0.2 %, V217 and V271 remained as clusters while V331 nucleated into a PDL. As illustrated by solid lines in Fig. 3(b), the influence of tensile strain on the formation energy of a cluster is not considerable. In contrast, the applied strain strongly influences the formation energy of PDLs. If we apply a larger compressive strain, we can generate PDLs from small VCs and those PDLs stably exist at a smaller compressive strain after structural relaxation by the CG method.

Those formation energies are indicated by dotted line in Fig. 3. Under zero strain, both a VC and PDL can exist for $19 \leq N_i \leq 169$. It can noticed that the formation energy of the PDL is influenced by applied strain, because the formation energy was computed for the system pre-relaxed before introducing the defects. After introducing the defects cell size was fixed during the minimization for the case of VC and PDL. As for NEB calculation we conserved the cell length during the minimization. Therefore, more strain energy is stored in the case of PDL. The strain can be estimate as $\varepsilon'_{\text{estimated}} = |b|/L_z \times A_{\text{PDL}}/L_x \times L_y = 1.2 \times 10^{-7} \times A_{\text{PDL}}$, where A_{PDL} is area of PDL which can be expressed as $A_{\text{PDL}} = l^2/4\pi$ .The strain is about 0.015 % for largest loop arround 4 nm diameter. Accordingly, the actual strain value for the PDL will be $\varepsilon'_{\text{estimated}} + \varepsilon_{\text{applied}}$, therefore in the case of PDL influence of actual strain on formation energy can be noticed. However, the added strain is very small compared with $\varepsilon_{\text{applied}}$ and will not affect the later part of discussion.

As shown in Fig. 4, spherical VCs (3D-VCs) are more stable as size increases. Whereas energy difference for smaller sizes (≤37) is considerably less. Further, transition from 3D-VC to PDL is challenging as it involves the diffusion with the movement of many atoms, whereas transition between 2D-VC and PDL, as studied in this paper, only requires a small displacement and does not necessitate the diffusion of atoms to achieve stability. 3D-VCs shown with closed symbols (■) have spherical structure, and they have low formation energies. However, asymmetrical 3D-VCs with higher formation energies exist at the intermediate VC sizes. As indicated in Fig. 4-subplot, we suppose that 2D-VCs

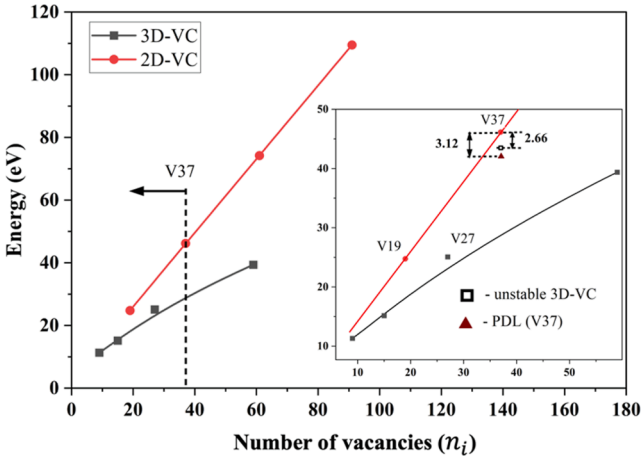

Fig. 4. The comparison of formation energy of spherical VC (3D-VC) vs planer VC (2D-VC).

can be formed from unstable or asymmetrical clusters. The 3D-VCs may transform into PLD and additional vacancies during this transition. However, this transition needs to be clarified by using dynamics simulations, and it is left for further study.

4. Energy barrier for the transition between VC and PDL

When a VC and PDL can exist at a given strain and vacancy size, it is considered that the transition between VC and PDL (VC–PDL transition) occurs with the help of thermal activation. Table 2 and 3 summarize the energy barrier for the VC–PDL transition calculated for symmetrical hexagonal and elongated hexagonal VCs. First, we discuss the activation energy without strain. Larger VCs (>V127) are nucleated into a corresponding PDL with almost zero energy barrier. For a cluster size less than or equal to V91, an energy barrier exists for this transition. Further, it was found that as VC size decreases, the energy barrier for the VC to PDL transition increases. If a planar VC with size V37 or larger is formed, or a small VC grows up to V37, the VC easily transforms to the corresponding PDL at room temperature since the energy barrier is 0.68 eV. Once the VC is transformed to the PDL, it acquires high mobility.

Table 2
Energy barriers of VC–PDL transitions as a function of compressive and tensile strain for symmetrical hexagonal shapes.

Boundary conditions		Activation energy (eV)											
		V19 to PDL		V37 to PDL		V61 to PDL		V91 to PDL		V127 to PDL		V169 to PDL	
		(→)	(←)	(→)	(←)	(→)	(←)	(→)	(←)	(→)	(←)	(→)	(←)
Tensile strain	**2.0 %**	5.65	0	7.40	0.95	-	-	-	-	-	-	-	-
	0.8 %	3.22	0.02	2.99	2.19	2.29	3.82	2.07	17.30	2.19	31.87	1.62	50.17
	0.6 %	2.85	0.09	2.38	2.52	1.60	4.74	1.35	19.43	1.17	34.98	1.42	55.52
	0.4 %	2.49	0.19	1.74	2.84	0.96	5.70	0.91	21.82	0.42	38.31	0.50	60.26
	0.2 %	2.06	0.23	1.09	3.15	0.54	6.89	0.30	24.00	0.37	42.29	0	65.33
zero stress		1.69	0.33	0.68	3.70	0.39	8.32	0.27	26.75	0	45.90	0	70.77
Compressive strain	**0.2 %**	1.31	0.43	0.45	4.42	0.14	9.65	0	29.23	–	–	–	–
	0.4 %	0.92	0.49	0.34	5.27	0	11.07	–	–	–	–	–	–
	0.6 %	0.56	0.60	0.14	6.02	–	–	–	–	–	–	–	–

Table 3
Energy barriers of VC–PDL transitions as a function of compressive and tensile strain for V29 elongated hexagonal shape.

Boundary conditions		Activation energy (eV)	
		V29 to PDL	
		(→)	(←)
Tensile strain	**2.0 %**	7.21	0.47
	0.8 %	3.37	0.61
	0.6 %	2.76	0.74
	0.4 %	2.25	0.98
	0.2 %	1.65	1.14
zero stress		1.16	1.40
Compressive strain	**0.2 %**	0.66	1.66
	0.4 %	0.41	2.17
	0.6 %	0.27	2.79

On the other hand, once a PDL with size V37 or larger is formed by deformation or transition from a corresponding VC, it stably exists as a PDL since the energy barrier for the transition is quite high (≥ 3.70 eV). Similarly, the energy barrier computed for the V29 to PDL transition is 1.16 eV, and the corresponding PDL to VC transition is 1.40 eV. Thus, if a PDL with V29 size is formed, it stably exists as PDL. However, the energy barrier computed for the V19 to PDL transition is 1.69 eV, and the corresponding PDL to VC transition is 0.33 eV. Thus, if a PDL with V19 size or smaller is formed, it easily transforms to a VC and loses mobility, except at higher temperature.

Fig. 5 shows how the tension/compression influences the transition energy barrier for the VC to PDL for V61. The energy barrier decreases under compression, becoming almost zero at 0.4 % compression. On the other hand, the energy barrier increases almost linearly with tensile strain. The energy barrier becomes 1.60 eV (see Table 2) under 0.6 % tension. The applied strain strongly influences the transition rate between a VC and PDL for small sizes. The transition of PDLs of V91 or larger to the corresponding VC is quite difficult (greater than3.82 eV, even at 0.8 % for V91). This implies that once a larger PDL is nucleated or smaller PDLs collide and become a larger PDL, they stay stable as PDLs rather than return to their corresponding VCs, even under strain.

Fig. 6 depicts the activation energies obtained by NEB calculations under strains for V19 (Fig. 6(a)), V29 (Fig. 6(b)), and V37 (Fig. 6(c)). As discussed earlier, V19 to the corresponding PDL is not easy without strain because of the high activation energy, whereas 0.4 % compressive strain reduces the energy barrier to 0.92 eV (also see Table 2). Further, around 0.6 % compressive strain makes the transition to PDL easier with the lower energy barrier of 0.56 eV. The transition from PDL to VC is relatively easy for all strain calculated in this study, but it becomes difficult under the compressive side.

The crossover occurs around 0.6 % compressive strain and, at the 0.6 % compressive strain, the transition from PDL to VC is more difficult than the opposite transition and the PDL becomes stable for a 0.6 % or larger compressive strain. As discussed earlier, V29 to the corresponding PDL is not easy without strain because of the high activation energy,

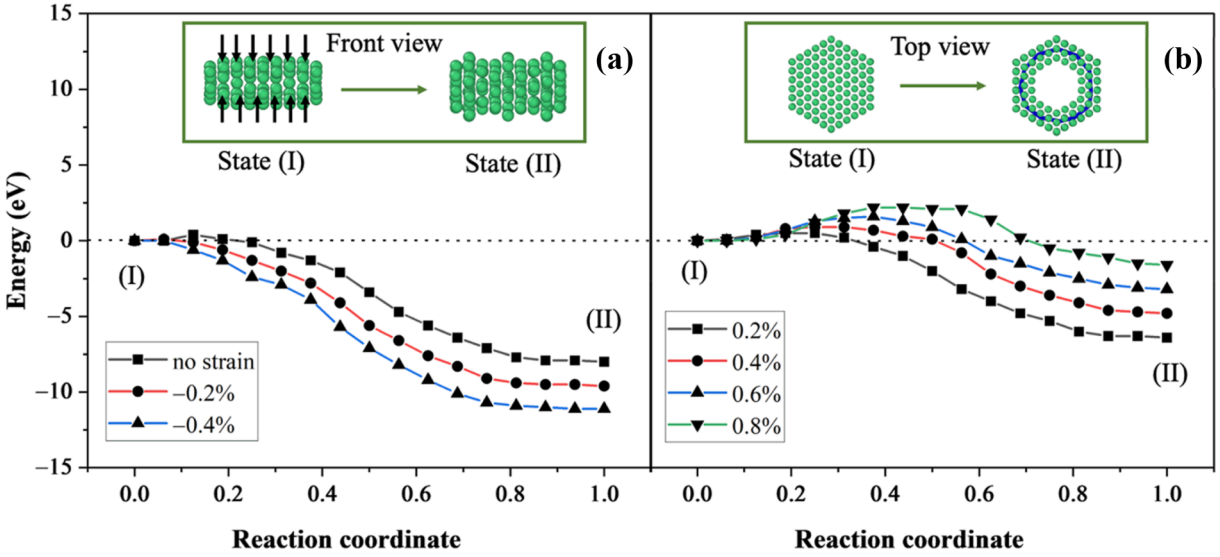

Fig. 5. NEB calculations of the enthalpy difference as a function of the reaction coordinate of V61 to a PDL for different values of applied strain: (a) compressive strain and (b) tensile strain.

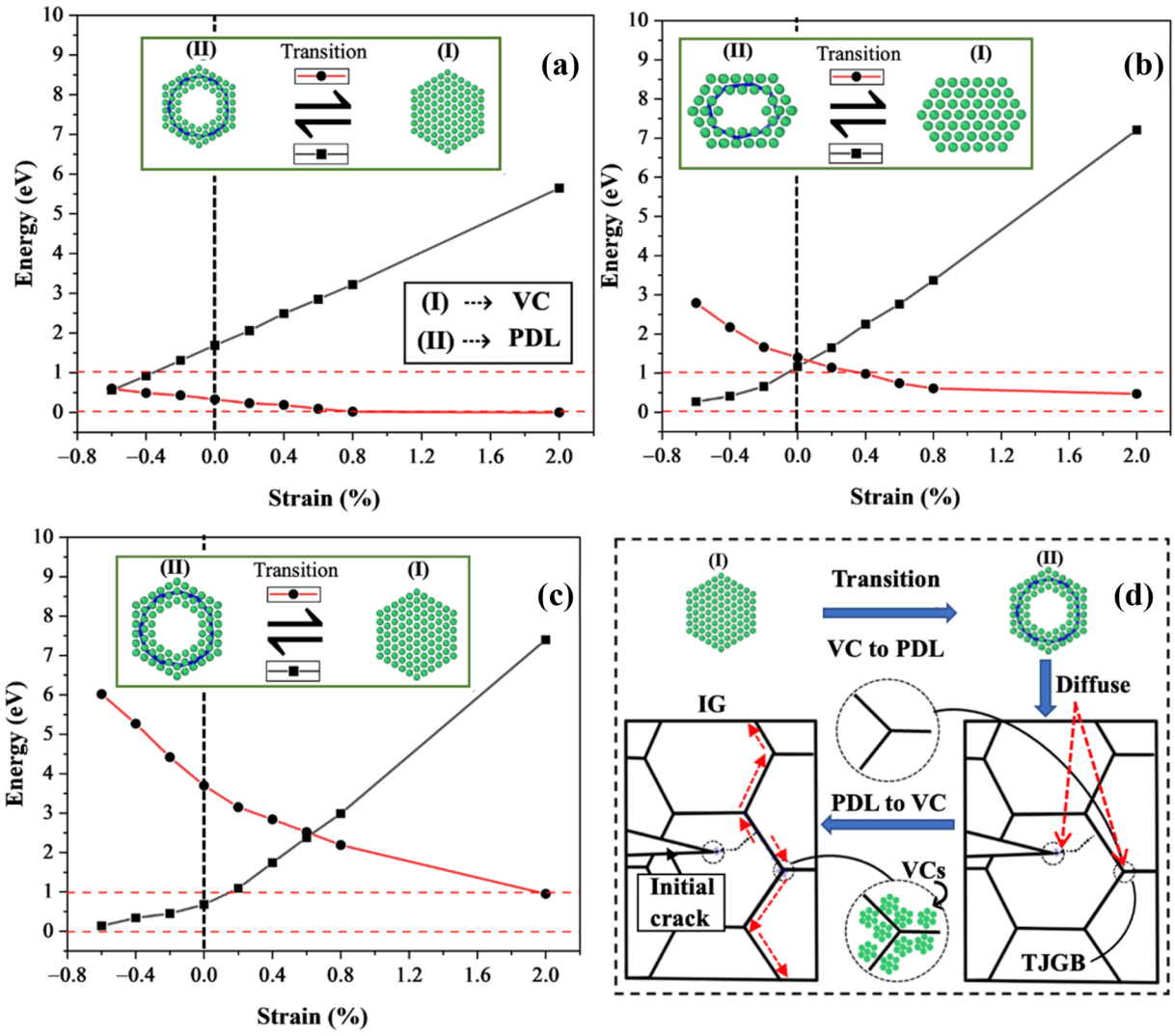

Fig. 6. PDL and VC transition stability under compressive/tensile strain for a (a) V19 symmetrical hexagonal VC, (b) V29 elongated hexagonal VC, (c) V37 symmetrical hexagonal VC, and (d) association with IG fracture mode.

whereas 0.2 % compressive strain reduces the energy barrier to 0.66 eV (also see Table 3).

Further, the VC to PDL transition is relatively easy for all compressive strains. The cross over occurs at a tensile strain less than 2 %, where at around 0.4 % tensile strain the PDL to VC transition becomes possible with the energy barrier of 0.98 eV. Further, around 2.0 % tensile strain reduces the energy barrier to 0.47 eV (also see Table 3). Therefore, V29 shows a good balance between the transition from VC to PDL under applied compressive/tensile strain. For V37, the energy barrier from VC to PDL almost reaches 0.14 eV at 0.6 % compressive strain, whereas for 0.8 % tensile strain it reaches 2.99 eV. The energy barrier for the opposite transition is 6.02 eV at 0.6 % compression, whereas it is 0.95 eV at 2 % tensile strain.

The cross over occurs at around 0.6 % tensile strain. The transition from PDL to VC is still difficult at 0.8 % tension at room temperature, but it is possible near a stress singularity, such as a crack tip or a triple junction of grain boundaries (TJGB) where 2 % tensile strain is realized. Under tensile stress, the cluster becomes more stable; in other words, the PDL will return to the corresponding VC when a tensile strain is applied, whereas it remains a PDL under compressive strain. PDLs easily cause one-dimensional (1D) thermal glide, whereas diffusion of VCs is quite difficult at room temperature. This means that high-speed vacancy transportation, from the compressive to tensile region, occurs though the PDL–VC transition and its stress dependency. As shown in Fig. 6(d), a VC formed under a hydrogen environment can nucleate into PDL or PDLs, which are directly formed under deformation, can diffuse to a region near a TJGB or GB and transform to a VC. These VCs can accumulate, with high-density VCs forming in the vicinity of GBs (a similar mechanism is possible near a crack tip as well). Detailed analyses of fracture surface morphologies of hydrogen-charged specimens have shown that many parts of hydrogen-related fractures are not exactly IG fractures, but they are transgranular fractures in the vicinity of GBs at the atomic scale [23]. This result indicates that priori accumulation of defects or hydrogen occurs. Further experimental verification is necessary, but the PDL–VC transition could be the assisting mechanism and may lead to IG-like fracture (or the accumulation of vacancies near a crack tip).

5. Conclusion

This study investigated the formation energy of regular and elongated hexagonal-shaped VCs and vacancy-type PDLs with Burgers vector 1/2 ⟨1 1 1⟩ in α-iron using MD simulation. Furthermore, the NEB method was applied to calculate the energy barrier for VC and PDL transitions without/with applied strain. Accordingly, the main findings are summarized as follows:

(1) The VC formation energy is not substantially influenced by the applied compressive/tensile strain. However, the transition condition and formation energy of PDLs strongly depend on the applied strain.
(2) The VC formation energy is proportional to its upper or bottom area and the PDL formation energy is proportional to its dislocation length.
(3) The transitions between VCs and PDLs under compressive/tensile strain conditions are possible for nano-sized VCs and PDLs where $N_i \leq 37$. For $N_i > 37$, the VC to PDL transition is possible, whereas the PDL to VC is not possible at room temperature.
(4) A PDL can easily cause 1D thermal glide, whereas VC diffusion is quite difficult at room temperature. This means that the high-speed vacancy transport from a compressive to tensile region and the vacancy accumulation at the tensile stress region occur due to the PDL–VC transition and its stress dependency.

This study concentrated on the transition between PDL and VC without hydrogen as explained in the introduction. When hydrogen atoms are trapped at PDL or VC, those atoms need to migrate to more stable positions during the transition between VC and PDL. The hydrogen effect needs to be clarified by using dynamics simulations, and it is left for further study.

Funding

This work was supported by ISIJ Research Group II “Extraction of essential factor technology for hydrogen embrittlement evaluation” and JSPS KAKENHI [Grant No 19H02025].

Data availability

The raw/processed data required to reproduce these findings cannot be shared at this time as the data also forms part of an ongoing study.

CRediT authorship contribution statement

Mugilgeethan VIJENDRAN: Conceptualization, Methodology, Software, Validation, Formal analysis, Writing – original draft. **Ryosuke MATSUMOTO:** Writing – review & editing, Supervision, Project administration, Funding acquisition.

Declaration of Competing Interest

The authors declare that they have no known competing financial interests or personal relationships that could have appeared to influence the work reported in this paper: [Ryosuke MATSUMOTO reports financial support was provided by Iron and Steel Institute of Japan. Ryosuke MATSUMOTO reports financial support was provided by Japan Society for the Promotion of Science.].

Data availability

Data will be made available on request.

References

[1] B. Johnston, M.C. Mayo, A. Khare, Hydrogen: the energy source for the 21st century, Technovation 25 (2005) 569–585, https://doi.org/10.1016/j.technovation.2003.11.005.
[2] R.L. Amaro, N. Rustagi, K.O. Findley, E.S. Drexler, A.J. Slifka, Modeling the fatigue crack growth of X100 pipeline steel in gaseous hydrogen, Int. J. Fatigue. 59 (2014) 262–271, https://doi.org/10.1016/j.ijfatigue.2013.08.010.
[3] G. Block, M.B. Rubin, J. Morris, J.G. Berryman, Simulations of dynamic crack propagation in brittle materials using nodal cohesive forces and continuum damage mechanics in the distinct element code LDEC, Int. J. Fract. 144 (2007) 131–147, https://doi.org/10.1007/s10704-007-9085-2.
[4] M. Nagumo, Fundamentals of hydrogen embrittlement, springer singapore, Singapore (2016), https://doi.org/10.1007/978-981-10-0161-1.
[5] H.K.D.H. Bhadeshia, Prevention of hydrogen embrittlement in steels, ISIJ Int. 56 (2016) 24–36.
[6] W.W. Gerberich, R.A. Oriani, M.J. Lji, X. Chen, T. Foecke, The necessity of both plasticity and brittleness in the fracture thresholds of iron, Philos. Mag. A Phys. Condens. Matter, Struct. Defects Mech. Prop. 63 (1991) 363–376, https://doi.org/10.1080/01418619108204854.
[7] H.K. Birnbaum, P. Sofronis, Hydrogen-enhanced localized plasticity—a mechanism for hydrogen-related fracture, Mater. Sci. Eng. A. 176 (1994) 191–202, https://doi.org/10.1016/0921-5093(94)90975-X.
[8] M. Nagumo, Hydrogen related failure of steels - a new aspect, Mater. Sci. Technol. 20 (2004) 940–950, https://doi.org/10.1179/026708304225019687.
[9] M.R. Louthan, Hydrogen embrittlement of metals: a primer for the failure analyst, J. Fail. Anal. Prev. 8 (2008) 289–307, https://doi.org/10.1007/s11668-008-9133-x.
[10] E. Hayward, C.-C. Fu, Interplay between hydrogen and vacancies in <math display=“inline”> <mi>α</mi> </math> -Fe, Phys. Rev. B. 87 (2013), 174103, https://doi.org/10.1103/PhysRevB.87.174103.
[11] L. Chiari, M. Fujinami, Recent Studies of Hydrogen-related Defects in Iron-based Materials, ISIJ Int. 62 (2022) 832–839, https://doi.org/10.2355/isijinternational.isijint-2021-422.
[12] M. Marinica, F. Willaime, N. Mousseau, Energy landscape of small clusters of self-interstitial dumbbells in iron 094119 (2011) 1–14, https://doi.org/10.1103/PhysRevB.83.094119.
[13] Z. Yao, M.L. Jenkins, M. Hernández-Mayoral, M.A. Kirk, The temperature dependence of heavy-ion damage in iron: a microstructural transition at elevated temperatures, Philos. Mag. 90 (2010) 4623–4634, https://doi.org/10.1080/14786430903430981.
[14] J. Marian, B.D. Wirth, A. Caro, B. Sadigh, G.R. Odette, J.M. Perlado, T. Diaz de la Rubia, Dynamics of self-interstitial cluster migration in pure α-Fe and Fe-Cu alloys, Phys. Rev. B. 65 (2002), 144102, https://doi.org/10.1103/PhysRevB.65.144102.
[15] Y.N. Osetsky, D.J. Bacon, A. Serra, B.N. Singh, S.I. Golubov, One-dimensional atomic transport by clusters of self-interstitial atoms in iron and copper, Philos. Mag. 83 (2003) 61–91, https://doi.org/10.1080/0141861021000016793.
[16] J. Fikar, R. Gröger, Shape of small prismatic dislocation loops in tungsten and iron, Solid State Phenom. 258 SSP (2017) 97–101, https://doi.org/10.4028/www.scientific.net/SSP.258.97.
[17] Y.N. Osetsky, M. Victoria, A. Serra, S.I. Golubov, Computer simulation of vacancy and interstitial clusters in bcc and fcc metals 1 (1997) 34–48.
[18] B.D. Wirth, G.R. Odette, D. Maroudas, G.E. Lucas, Dislocation loop structure, energy and mobility of self-interstitial atom clusters in bcc iron, J. Nucl. Mater. 276 (2000) 33–40, https://doi.org/10.1016/S0022-3115(99)00166-X.
[19] J. Gao, E. Gaganidze, J. Aktaa, Parameterization on formation free energy of dislocation loops up to 1100 K in bcc iron, J. Nucl. Mater. 559 (2022), 153409, https://doi.org/10.1016/j.jnucmat.2021.153409.
[20] J.R. Beeler, R.A. Johnson, Vacancy clusters in α-iron, Phys. Rev. 156 (1967) 677–684, https://doi.org/10.1103/PhysRev.156.677.
[21] C.C. Matthai, D.J. Bacon, The collapse of vacancy clusters a molecular dynamics study, J. Nucl. Mater. 135 (1985) 173–180, https://doi.org/10.1016/0022-3115(85)90075-3.
[22] J. Fikar, R. Schäublin, D.R. Mason, D. Nguyen-manh, Nano-sized prismatic vacancy dislocation loops and vacancy clusters in tungsten, Nucl. Mater. Energy. 16 (2018) 60–65, https://doi.org/10.1016/j.nme.2018.06.011.
[23] A. Shibata, T. Murata, H. Takahashi, T. Matsuoka, N. Tsuji, Characterization of hydrogen-related fracture behavior in as-quenched low-carbon martensitic steel and tempered medium-carbon martensitic steel, Metall. Mater. Trans. A. 46 (2015) 5685–5696, https://doi.org/10.1007/s11661-015-3176-x.
[24] T. Neeraj, R. Srinivasan, J. Li, Hydrogen embrittlement of ferritic steels: observations on deformation microstructure, nanoscale dimples and failure by nanovoiding, Acta Mater. 60 (2012) 5160–5171, https://doi.org/10.1016/j.actamat.2012.06.014.
[25] J. Kameda, Equilibrium and growth characteristics of hydrogen-induced intergranular cracking in phosphorus-doped and high purity steels, Acta Metall. 34 (1986) 1721–1735, https://doi.org/10.1016/0001-6160(86)90119-7.
[26] M. Nagumo, K. Takai, The predominant role of strain-induced vacancies in hydrogen embrittlement of steels: Overview, Acta Mater. 165 (2019) 722–733, https://doi.org/10.1016/j.actamat.2018.12.013.
[27] Y. Ding, H. Yu, M. Lin, K. Zhao, S. Xiao, A. Vinogradov, L. Qiao, M. Ortiz, J. He, Z. Zhang, Hydrogen-enhanced grain boundary vacancy stockpiling causes transgranular to intergranular fracture transition, Acta Mater. 239 (2022), 118279, https://doi.org/10.1016/j.actamat.2022.118279.
[28] A.P. Thompson, H.M. Aktulga, R. Berger, D.S. Bolintineanu, W.M. Brown, P. S. Crozier, P.J. in ’t Veld, A. Kohlmeyer, S.G. Moore, T.D. Nguyen, R. Shan, M. J. Stevens, J. Tranchida, C. Trott, S.J. Plimpton, LAMMPS - a flexible simulation tool for particle-based materials modeling at the atomic, meso, and continuum scales, Comput. Phys. Commun. 271 (2022), 108171, https://doi.org/10.1016/j.cpc.2021.108171.
[29] M. Wen, A new interatomic potential describing Fe-H and H-H interactions in bcc iron, Comput. Mater. Sci. 197 (2021), 110640, https://doi.org/10.1016/j.commatsci.2021.110640.
[30] G.J. Ackland, M.I. Mendelev, D.J. Srolovitz, S. Han, A.V. Barashev, Development of an interatomic potential for phosphorus impurities in -iron, J. Phys. Condens. Matter. 16 (2004) S2629–S2642, https://doi.org/10.1088/0953-8984/16/27/003.

[31] D. Terentyev, D.J. Bacon, Y.N. Osetsky, Interaction of an edge dislocation with voids in α-iron modelled with different interatomic potentials, J. Phys. Condens. Matter. 20 (2008), 445007, https://doi.org/10.1088/0953-8984/20/44/445007.
[32] X.D. Pan, T. Lu, Y.M. Lyu, Y.P. Xu, H.S. Zhou, Z.S. Yang, G.J. Niu, X.C. Li, F. Gao, G. N. Luo, Effect of H on the formation of vacancy dislocation loops in α-Fe, J. Nucl. Mater. 542 (2020), 152500, https://doi.org/10.1016/j.jnucmat.2020.152500.
[33] A. Stukowski, K. Albe, Extracting dislocations and non-dislocation crystal defects from atomistic simulation data, Model. Simul. Mater. Sci. Eng. 18 (2010), https://doi.org/10.1088/0965-0393/18/8/085001.